JOURNAL OF MATERIALS SCIENCE 30 (1995) 643–654

Cyclic fatigue in monolithic alumina: mechanisms for crack advance promoted by frictional wear of grain bridges

C.J. GILBERT, R.N. PETRANY, R.O. RITCHIE
Department of Materials Science and Mineral Engineering, University of California, Berkeley, CA 94720, USA

R.H. DAUSKARDT
Department of Materials Science and Engineering, Stanford University, Stanford, CA 94305, USA

R.W. STEINBRECH
Institute for Materials in Energy Systems, Forschungszentrum Jülich GmbH, D52425 Jülich, Germany

The microstructural basis of cyclic fatigue-crack propagation in monolithic alumina has been investigated experimentally and theoretically. A true cyclic fatigue effect has been verified, distinct from environmentally assisted slow crack growth (static fatigue). Microstructures with smaller grain sizes were found to promote faster crack-growth rates; growth rates were also increased at higher load ratios (i.e. ratio of minimum to maximum applied loads). Using *in situ* crack-path analysis performed on a tensile loading stage mounted in the scanning electron microscope, grain bridging was observed to be the primary source of toughening by crack-tip shielding. In fact, crack advance under cyclic fatigue appeared to result from a decrease in the shielding capacity of these bridges commensurate with oscillatory loading. It is proposed that the primary source of this degradation is frictional wear at the boundaries of the bridging grains, consistent with recently proposed bridging/degradation models, and as seen via fractographic and *in situ* analyses; specifically, load versus crack-opening-displacement hysteresis loops can be measured and related to the irreversible energy losses corresponding to this phenomenon.

1. Introduction

Unlike metals, ceramics have traditionally been considered to be immune to fatigue damage under cyclic loading, a notion justified by the low mobility of dislocations in ceramic materials and corresponding lack of crack-tip plasticity [1]. Despite several early observations to the contrary [2–6], crack advance observed under cyclic loading was commonly attributed to environmentally assisted growth (static fatigue or stress-corrosion cracking) integrated over the loading cycle [7]. Over the last several years, however, there have been numerous demonstrations of a true cyclic fatigue effect in many polycrystalline ceramics; specifically, at equivalent stress-intensity levels, rates of subcritical crack growth under cyclic loads at ambient temperatures have been shown to be far in excess of those measured under quasi-static loads [8–16]. The dominant microstructural mechanisms, however, remain poorly understood, and quantitative descriptions of such behaviour are generally lacking.

Although most "high-toughness" ceramics are known to develop toughness through resistance or *R*-curve behaviour [17–22], where mechanisms such as *in situ* phase transformations [21], crack bridging [18, 19, 22], or microcracking [20] act to locally *shield* the crack tip from applied stresses, it has become apparent that the degradation of such toughening mechanisms (particularly bridging) under cyclic loading may promote fatigue-crack growth [23, 24]. For example, in many nontransforming ceramics, the principal contribution to toughening arises from crack bridging, whether by uncracked ligaments at interlocking grains in monolithic systems such as Al_2O_3 and Si_3N_4 [25–31] or by intact whiskers, fibres or particles in many composite structures [32, 33]. Effective bridging in monolithic ceramics relies not only on sufficiently weak grain boundaries but also on thermal expansion anisotropy which leaves some grains in a state of residual compression after cooling from processing temperatures [19, 27, 34]. (Large radial compressive stresses can similarly be imposed on the fibre or whisker/matrix interface in many composite microstructures.) Upon encountering such compressive zones, a crack will tend to deflect around the grain in the tensile regions surrounding it, thereby leaving

0022–2461

TABLE I Properties of alumina ceramics

Al_2O_3	Purity (%)	Grain size, d_{gs} (μm)	Young's modulus, E (GPa)	Bend strength, σ_0 (MPa)	Initiation toughness, K_0 (MPa $m^{1/2}$)	Maximum measured toughness, K_c (MPa $m^{1/2}$)
Al_2O_3-Coors I	99.5	[a]	370	260	–	5.1
Al_2O_3-Coors II	95.5	[a]	–	–	–	5.3
Al_2O_3-I	98.8	8	340	193	2.5	3.7[b]
Al_2O_3-II	98.5	10	365	–	2.5	4.4[b]
Al_2O_3-III	–	13	380	–	2.5	5.3[b]

[a] Highly non-uniform grain structures, with grains ranging in size from 2–30 μm.
[b] Owing to large-scale bridging, these values represent the maximum measured toughness.

an intact grain traversing the crack faces to act as a local bridge. Toughening then results from closing tractions acting across the crack flanks during both initial debonding of the grain and subsequent frictional grain pullout.

During cyclic loading, however, it is presumed that the shielding capacity of the bridging zone is reduced due to frictional wear degradation at the grain/matrix interface. This notion is supported by indirect evidence, such as the appearance of wear debris at active bridge/matrix boundaries [24, 30], as well as subtle rounding, debris products, and wear tracts observed on otherwise identical fatigue fracture surfaces [35]. The essential difference between static and cyclic fatigue-crack growth is therefore associated with an increase in the local crack-tip driving force under cyclic loads. This, in turn, suggests that the actual crack-tip advance mechanism may be identical during cyclic and static crack extension.

Recent micro-mechanical modelling [23, 24] has shown that repetitive sliding wear of frictional grain bridges under cyclic loading can result in premature debonding of grains and reduced frictional pullout stresses, factors which markedly reduce the toughening capacity of grain-bridging zones in cyclic fatigue; similar mechanisms are apparent for frictional bridging by partially bonded whiskers or fibres in composite microstructures [36]. Such frictional-wear models not only permit calculation of fatigue-crack growth rate behaviour for ceramics, but also predict growth rates to be markedly sensitive to the applied stress intensity and to microstructural and mechanical parameters such as grain size and residual stress.

The objective of the present study was to examine the cyclic fatigue-crack growth behaviour of a monolithic alumina, which shows significant R-curve toughening by grain bridging. It is shown that a frictional wear model for crack advance provides an accurate description of experimentally observed behaviour in several aluminas with varying grain size and processing conditions.

2. Experimental procedures

2.1. Materials

Five grades of monolithic alumina were examined, namely two Coors commercial-grade materials (one with a purity of 99.5%, a highly non-uniform grain size distribution, and a steady-state or plateau fracture toughness, K_c, of 5.1 MPa $m^{1/2}$, the other with a purity of 95.5%, a highly non-uniform grain size distribution, and a K_c of 5.3 MPa $m^{1/2}$), and three grades processed by isostatically pressing high-purity Al_2O_3 powders at 1700 °C *in vacuo*. The latter three microstructures, which consisted of highly equiaxed grain structures with grain sizes of approximately 8, 10 and 13 μm, displayed significant R-curve behaviour, with crack-initiation fracture toughness K_0 values of ~ 2.5 MPa $m^{1/2}$ and K_c values of 3.7, 4.4 and 5.3 MPa $m^{1/2}$, respectively. Specific properties of all five grades are listed in Table I; characteristic microstructures (for the two Coors materials and the 13 μm material) are shown in Fig. 1.

2.2. Cyclic crack-growth rate and closure measurements

Cyclic crack-growth rate measurements were performed using compact-tension, C(T), specimens, containing "long" ($\gtrsim 3$ mm) through-thickness cracks, in a controlled room-air environment (22 °C, 45% relative humidity). Test pieces conformed to ASTM standard geometry, with a width, W, of 20 mm and a thickness of 3 mm. Specimens were cycled at load ratios ($R = K_{min}/K_{max}$) of 0.1 and 0.5 at a cyclic frequency of $\nu = 25$ Hz (sine wave) on computer-controlled servohydraulic mechanical testing machines, in general accordance with ASTM standard E647-91, modified for ceramics using procedures described elsewhere [37]. Prior to data collection, samples were pre-cracked under cyclic loading several millimetres beyond the wedge-shaped starter-notch; thereafter, crack lengths were continuously monitored (to within ± 2 μm) using electrical-potential measurements across thin (~ 100 nm) NiCr films evaporated on to the specimen surface. Measurements were checked periodically with a travelling microscope in order to minimize errors resulting from bridging-induced electrical contact behind the crack tip in the NiCr crack gauge. Data are presented in terms of the growth rate per cycle, da/dN, as a function of either the maximum or alternating applied stress intensity, K_{max} or ΔK ($= K_{max} - K_{min}$), respectively. Selected specimens were subsequently loaded monotonically at loading rates of ~ 0.25 μm s^{-1} to obtain resistance curves. Stress/life (S/N) data were also obtained in the 99.5%

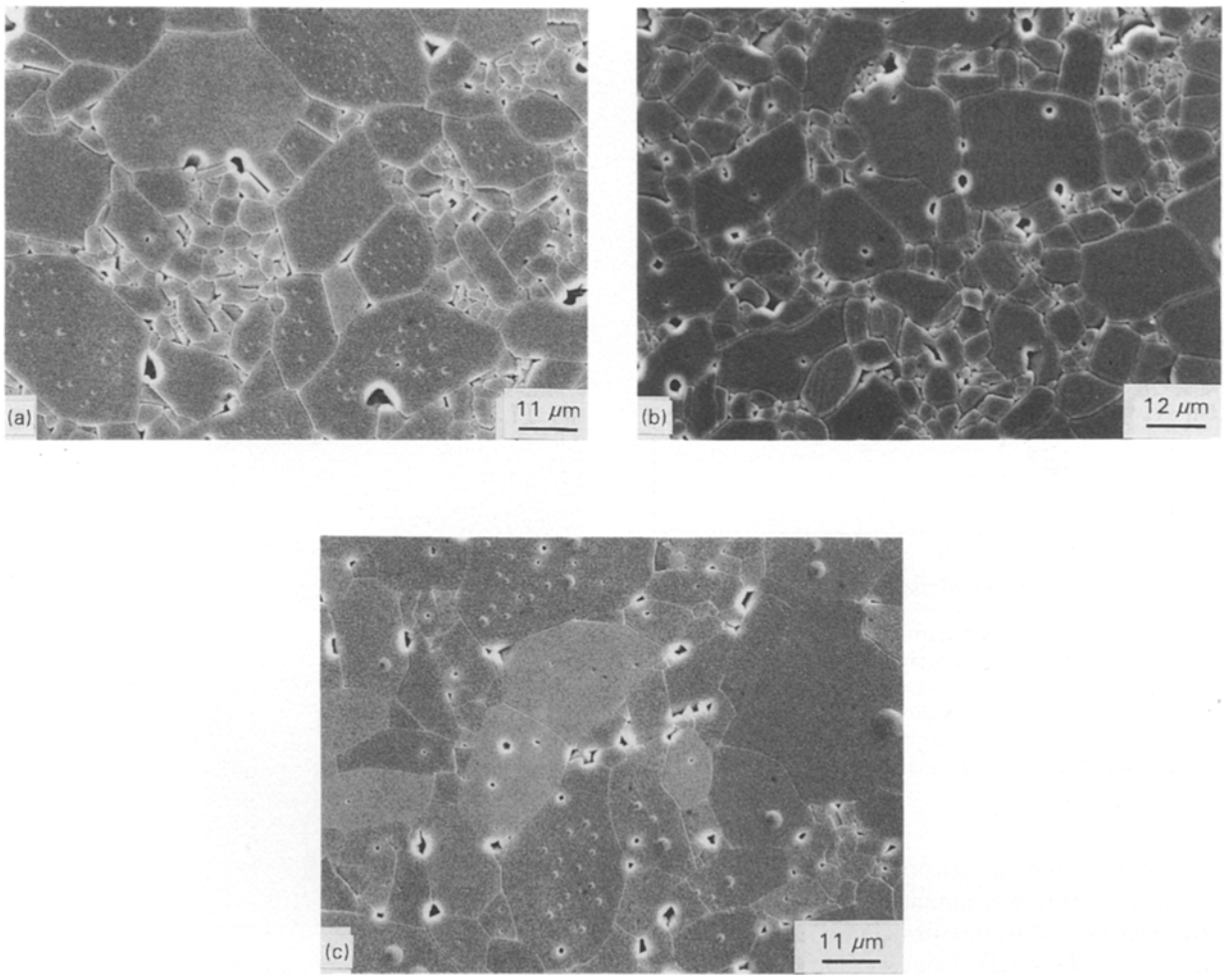

Figure 1 Representative microstructures for (a) the Coors 99.5% pure Al_2O_3, (b) the Coors 95.5% pure Al_2O_3, and (c) the 13 μm grain-sized Al_2O_3. Notice the largely non-uniform nature of the two Coors microstructures relative to the equiaxed structure of the 13 μm alumina. Each surface was prepared by thermally etching in air at 1650 °C for 2 h.

Coors alumina using a cantilever-beam specimen at a load ratio of $R = -1.0$. Fig. 2 schematically illustrates the experimental techniques used for crack growth-rate measurements.

Residual crack opening ("crack closure" in metals terminology), in the form of wedging contact of mating crack faces upon specimen unloading, was monitored in the 10 μm grain-sized alumina using back-face strain elastic compliance measurements from strain gauges attached to the back face of the C(T) specimens. The closure stress intensity, K_{cl}, defined at the point of first wedging contact of the crack surfaces during unloading, was estimated on load versus back-face strain curves at the point where the elastic unloading line deviated markedly from linearity (Fig. 2) [38].

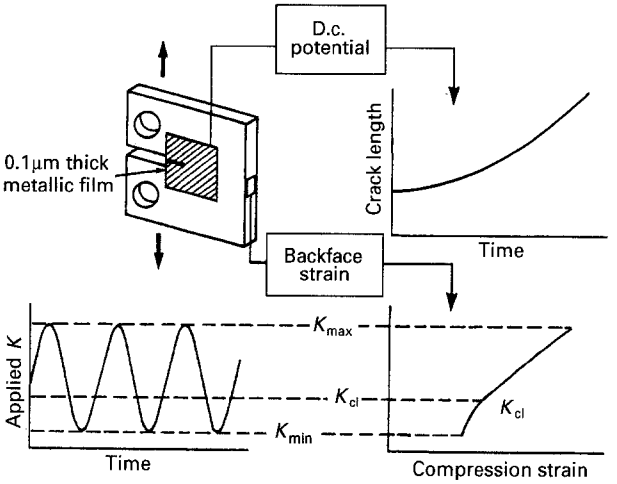

Figure 2 Experimental techniques used to measure cyclic fatigue-crack growth rates of "long" through-thickness cracks, showing compact-tension, C(T), specimen and procedures used to monitor crack length and the stress intensity at crack closure, K_{cl}.

2.3. *In situ* crack-path analysis and fractography

Fracture surfaces of samples tested under both monotonic and cyclic loads were examined in the scanning electron microscope (SEM). In addition, crack profiles in a series of C(T) specimens were imaged in the SEM using an *in situ* miniature screw-driven tensile loading stage, which permitted measurements of the local crack-opening displacement, $2u$, as a function of applied load, P, in the microscope.

3. Results and discussion

3.1. Resistance curve behaviour

Typical resistance curves for the 8 and 13 μm grain-sized microstructures are plotted in Fig. 3 in the form of the resistance to crack extension, K_R, as a function of normalized crack length, a/W, where W is the

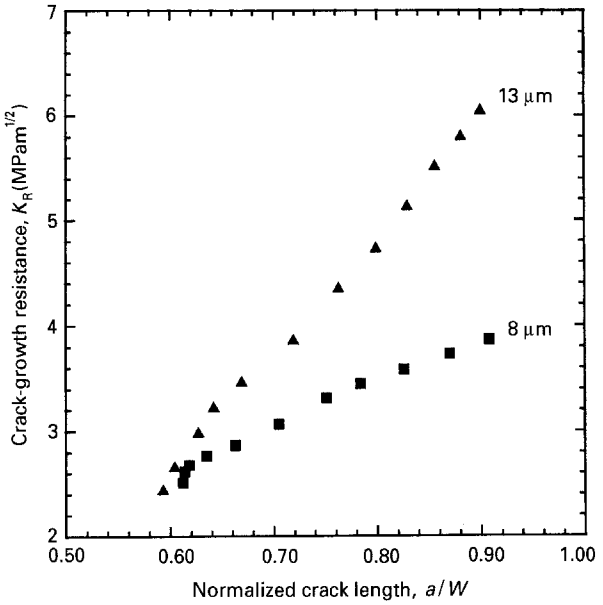

Figure 3 Plot of crack-growth resistance (*R*-curves) for the 8 and 13 μm grain-sized microstructures, plotted in terms of crack-growth resistance, K_R, as a function of normalized crack extension, a/W. Note the general increase in crack-growth resistance with increasing grain size, attributed to enhanced shielding due to larger grain-bridging zones which scale with grain size.

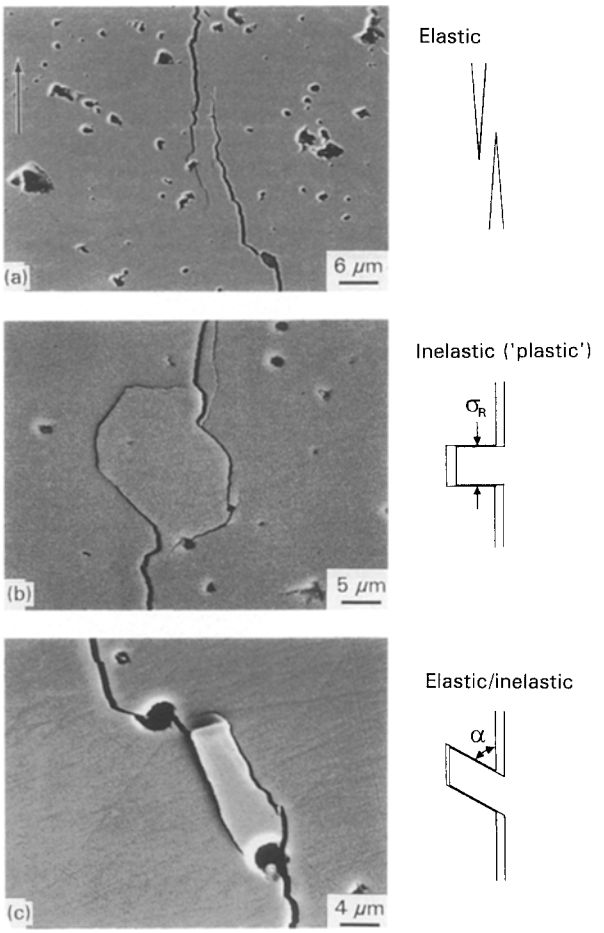

Figure 4 Examples of types of crack bridging in the Coors 95.5% alumina, showing (a) intact elastic bridges, (b) frictionally sliding inelastic bridges, and (c) mechanically interlocked elastic/inelastic bridges. (Classification after [22].)

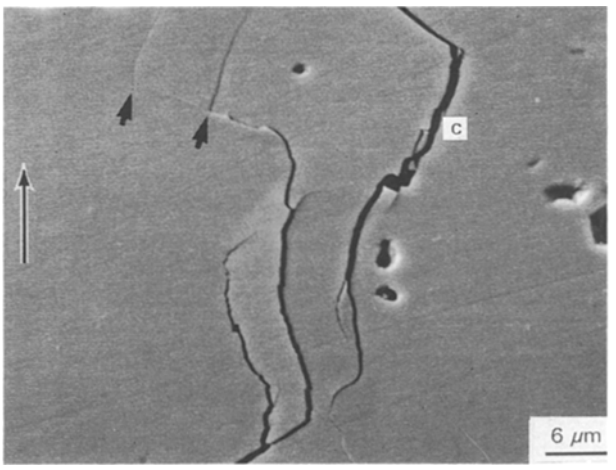

Figure 5 Evidence of extensive crack bifurcation in the crack wake of the Coors 95.5% alumina. Note the regions of secondary cracking (labelled with small arrows) opened under the operation of frictional tractions acting along the mating crack surfaces. The primary crack is labelled c. Large arrow indicates direction of crack growth.

width of the compact-tension specimen and a the crack length; these measurements indicate an increase in crack-growth resistance (toughness) with increasing grain size, as observed previously [17, 19, 25–28]. The elevation in toughness was found to be associated with crack bridging, involving the formation of unbroken ligaments (Fig. 4a), and in particular the development of extensive intact grain bridges behind the crack tip (Fig. 4b and c). Regions of crack bifurcation and secondary cracking were also observed, although less frequently, in the crack wake (Fig. 5); arrows in this figure mark regions where frictional tractions along the mating surfaces have opened new secondary cracks not associated with the primary crack (labelled C).

Following the classification by Rödel [22], various types of crack-bridging geometries can be documented in the aluminas: intact elastic bridges, frictionally sliding inelastic bridges, and mechanically interlocked elastic–inelastic bridges (see schematic illustrations in Fig. 4). Intact elastic bridges are characterized by the reversible nature of their deformation, a property which renders them immune to degradation under cyclic loading conditions (Fig. 4a). Previous approximate calculations [27] demonstrate that these elastic bridges cannot fully account for the magnitude of the measured toughness. Inelastic bridges, as shown in Fig. 4b, result from frictional sliding at the grain/matrix interface. The frictional sliding resistance depends on the coefficient of friction, μ, of the interface and the normal stress, σ_N, acting across the interface. Typically, $\sigma_N = \sigma_R$, where σ_R represents the residual stress which arises from thermal expansion anisotropy. The work performed against these frictional grain-bridging forces on crack opening has been shown to account for the majority of the observed toughening [27]. Elastic–inelastic bridges, are essentially a combination of the two idealized cases above (Fig. 4c); these incorporate elastic, reversible deformation with irreversible frictional sliding behaviour,

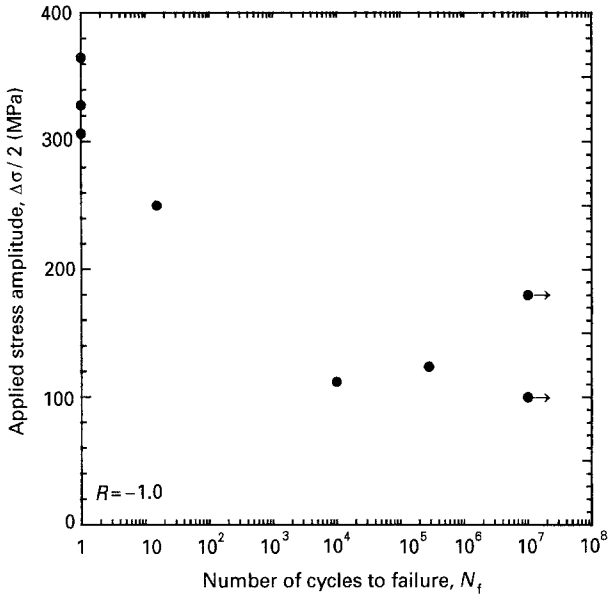

Figure 6 Stress/life (S/N) data, at $R = -1.0$, for the bimodal grain-sized alumina (99.5% purity), plotted in terms of the stress amplitude, $\Delta\sigma/2$, and cycles to failure, N_f.

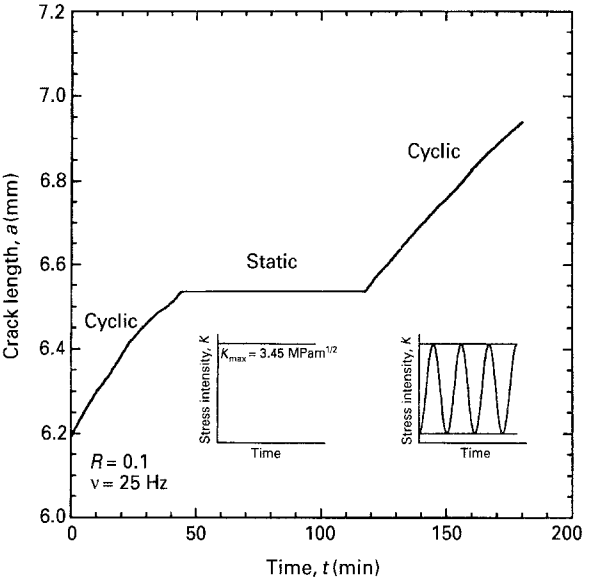

Figure 7 Crack length, a, plotted as a function of time, t, demonstrating the effect of sustained loading conditions versus cyclic loading conditions ($R = 0.1$, $\nu = 25$ Hz) in the Coors I alumina specimen. Notice the increase in growth rates under cyclic loading compared to those observed under sustained loading. The data are characteristic of each of the five alumina microstructures and demonstrate the presence of a true cyclic fatigue effect.

a combination which depends upon the tilt angle, α, of the bridge.

3.2. Cyclic fatigue

3.2.1. Stress/life behaviour

Typical stress/life (S/N) data for the Coors I alumina are shown in Fig. 6, where the applied stress amplitude, $\Delta\sigma/2$, is plotted as a function of cycles to failure, N, for a tension-compression loading schedule ($R = -1.0$, $\nu = 25$ Hz); arrows indicate tests interrupted prior to specimen failure at 10^7 cycles. These data are generally described by an equation of the form $\Delta\sigma^n N = C$, where n and C are scaling parameters. A least-squares fit to the data in Fig. 6 yields a value for n of 16.1, consistent with results reported elsewhere [39, 40].

3.2.2. Crack-growth behaviour

For the five alumina microstructures tested, rates of subcritical crack growth under cyclic loads were observed to exceed by far the corresponding growth rates under monotonic loading at equivalent stress-intensity levels, as shown in Fig. 7 for the Coors I alumina. Here crack length is plotted as a function of time for a series of block-loading experiments designed to distinguish cyclic and static fatigue effects. This is achieved by comparing growth rates at a constant applied stress intensity, K_{max}, to those measured under cyclic conditions at the same K_{max} (with $R = 0.1$).

Cyclic fatigue-crack growth-rate data (da/dN versus ΔK) measured over four orders of magnitude are plotted in Fig. 8a for all five alumina microstructures at $R = 0.1$ and $\nu = 25$ Hz. Similar to metallic materials over the mid-range of growth rates, these data may be expressed in terms of a simple Paris-law relationship of the form [41]

$$da/dN = C(\Delta K)^m \quad (1)$$

where C and m are scaling constants. The exponents, m, listed in Table II, are far higher than those reported for metallic systems (where m typically lies between 2 and 4) [8]; values of C and the fatigue threshold, ΔK_{th} (defined at a maximum growth rate of 10^{-10} m cycle^{-1}) are also tabulated. For the high-purity isostatically-pressed aluminas, growth rates are seen to increase, and fatigue thresholds appear to decrease, with both decreasing grain size, d_{gs}, and toughness, K_c; in fact, similar to many ceramic materials [8], the growth-rate behaviour for all alumina microstructures can be normalized by plotting as a function of K_{max}/K_c (Fig. 8b).

Cyclic fatigue behaviour has been modelled [23] in terms of a reduction in the grain-bridging stress function, $p(u)$, used to characterize crack surface closing tractions developed in the bridging zone (Fig. 9c); such a zone is schematically illustrated in Fig. 9a, with a representative $p(u)$ function under monotonic loading (Fig. 9b), where $2u$ is the crack-opening displacement. As grain debonding progresses under monotonic loading, $p(u)$ rises steeply from an initial compressive residual stress, σ_R, to a maximum tensile value representing complete detachment of the bridged grain from the surrounding matrix. This steady increase in $p(u)$ is followed by a gradual decrease dominated by frictional pullout (Fig. 9b), which is generally represented by a relationship of the form [23]

$$p(u) = \mu\sigma_N(1 - u/u^*), \quad (2)$$

where μ is the frictional coefficient and σ_N the normal stress acting on the bridge/matrix boundary

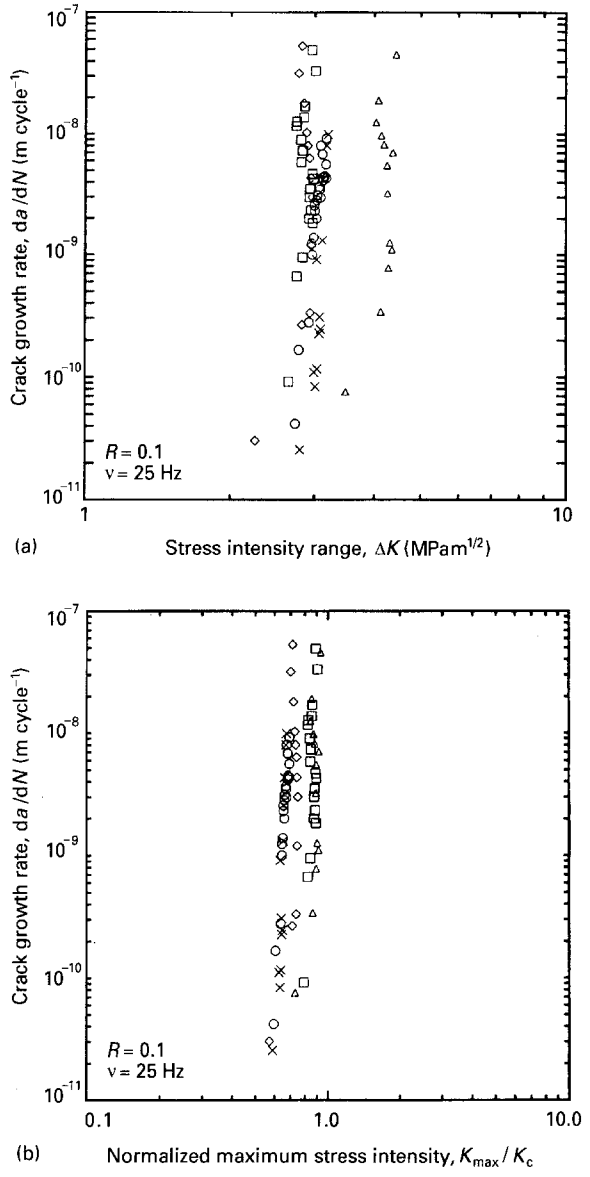

Figure 8 Effect of grain size on cyclic fatigue-crack growth rate behaviour in the five alumina microstructures as a function of (a) applied ΔK, and (b) K_{max}/K_c. (×) Coors II (○) Coors I, (□) 8 μm, (◇) 10 μm, (△) 13 μm.

TABLE II Paris-law parameters and fatigue thresholds for aluminas tested

Al_2O_3	m	C [(m cycle^{-1}) (MPa m$^{1/2}$)$^{-m}$]	Threshold ΔK_{th} (MPa m$^{1/2}$)
Al_2O_3-Coors I	32	5.5×10^{-56}	2.8
Al_2O_3-Coors II	47	6.1×10^{-33}	2.8
Al_2O_3-I	17	2.3×10^{-37}	2.7
Al_2O_3-II	16	1.1×10^{-36}	2.8
Al_2O_3-III	16	1.0×10^{-42}	3.9

(equivalent to the residual stress σ_R). The linear decrease in frictional stress with increasing u is modelled by the term $(1 - u/u^*)$, where u^* is the critical crack opening displacement at bridge rupture and is typically about half the grain size. A measure of the energy dissipated during frictional grain pullout is given by the area under the $p(u)$ function, where initial debonding (which consumes far less energy) is generally ignored [42]. The resultant increase in toughness, G_b, (i.e. the toughening capacity of the bridging zone) can be determined using energy-balance arguments [43]; moreover, the near-tip driving force, G_{tip}, is given by $G_{tip} = G_{app} - G_b$, where G_{app} represents the applied, far-field loading. Equivalently, this can be expressed in terms of stress intensities as

$$K_{tip} = (K_{app}^2 - K_b^2)^{1/2} \quad (3)$$

Accumulated wear damage at the bridge/matrix interface [23, 24, 30] results in a reduction in the toughening capacity of the bridging zone, K_b, under cyclic loads, leading to an increase in the crack-tip driving force, K_{tip}, (Equation 3).

Such analyses are consistent with *in situ* SEM observations of fatigue crack profiles. For example, the presence of irreversible deformation attributed to frictional wear can be seen in Fig. 10. When measuring the crack-opening displacement, $2u$, as a function of applied load, P, in the proximity of a frictionally sliding bridge ~ 2 mm behind the crack tip in a crack in the 13 μm alumina, extensive hysteresis was observed. The bridge is shown fully loaded at ~ 140 N in Fig. 10a, and unloaded in Fig. 10b, reflecting compliance changes resulting from a transition between elastic and inelastic deformation [14, 27]. Upon initial loading, bridges behave elastically until loads are sufficient to overcome frictional resistance at the bridge/matrix interface, whereupon they are pulled from their sockets; as sliding continues the stiffness is reduced below the elastic value. With subsequent unloading, the bridges first relax elastically, followed by frictional sliding as they return to their initial positions, resulting in a hysteresis curve. The area under this curve reflects irreversible energy losses per loading cycle which can be related to the shielding capacity of the bridging zone, G_b [27]. The idealized $p(u)$ behaviour shown in Fig. 10d is assumed to occur for individual bridging grains; it does not include the effects of neighbouring grains on the measured $p(u)$ curve shown in Fig. 10c.

Direct observation of the evolution of active bridging sites during cyclic loading suggests that this energy dissipation results from progressive elimination of the shielding capacity of bridging grains under the influence of oscillatory load. Fig. 11b shows the same bridging grain imaged in Fig. 11a (both at zero applied load), but after the application of $\sim 2 \times 10^6$ loading cycles at $R = 0.1$. There is clear evidence of damage to the bridge, involving micro-fracture and the removal of large particles; moreover, the secondary crack (indicated by the arrow) has closed relative to its position in Fig. 11a due to a reduction in the local frictional traction acting along this boundary.

Fractographic analysis of the Coors I Al_2O_3 (the 99.5% purity material) provides additional evidence of local bridge damage under cyclic loading. Unlike metals where fatigue surfaces exhibit striations associated with the unique mode of cyclic crack advance, both monotonic and cyclic fracture surfaces of the alumina in Fig. 12 show very similar intergranular morphologies. Such similarities are consistent with the notion

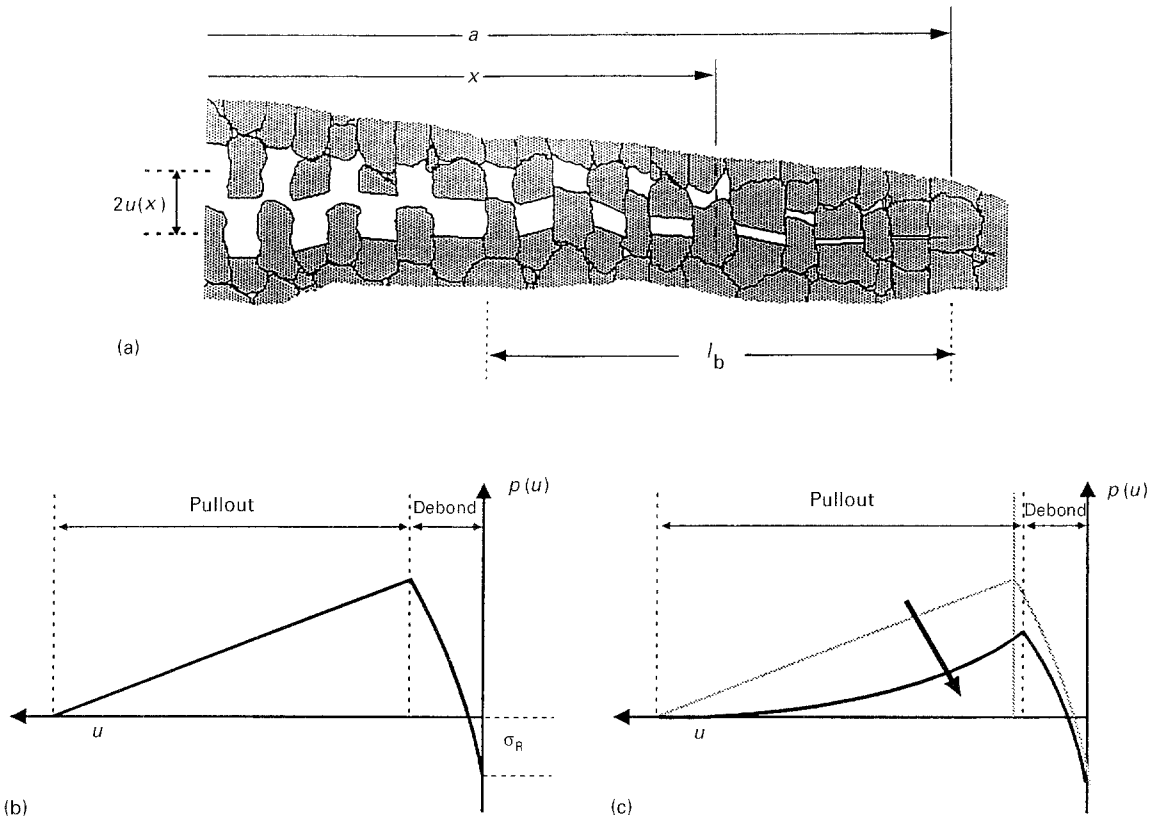

Figure 9 Grain bridges in the wake of a growing crack, length a, forming a bridging zone of length, l_b, are schematically illustrated in (a) [27]. The crack-opening displacement, $2u(x)$, is indicated at position x in the bridging zone. The grain bridging stress, $p(u)$, is shown rising rapidly from the initial residual compressive stress, σ_R, as the grain debonds, followed by frictional sliding which gradually decreases as the grain is extracted from the matrix under (b) monotonic, and (c) cyclic loading conditions. Note the marked decrease in $p(u)$ from wear at the grain/matrix interface under cyclic loading. After [23].

that the mode of crack advance is identical during cyclic and monotonic crack advance. However, evidence of wear damage on the cyclic fatigue surface is consistent with progressive reductions in the potency of grain-bridging phenomenon under cyclic loads.

Lathabai *et al.* [24] have modelled reduction of the bridging zone capacity in terms of a decrease in the frictional coefficient, μ, at the grain/matrix interface upon cyclic loading; the reduction in μ necessary to predict the observed behaviour is obtained by fitting the model to experimental stress/life (S/N) data. Alternatively, the degradation in $p(u)$ can be modelled directly in terms of the effect of material removed from the bridge/matrix interface by sliding wear processes on the residual thermal expansion anisotropy stress, σ_R (while maintaining the frictional coefficient, μ, at the boundary constant). In this approach [23], the normal stress, σ_N, acting across the sliding interface is taken to be the residual stress, σ_R, given by

$$\sigma_R \approx \frac{E}{2(1-\nu^2)}\varepsilon_r^* \tag{4}$$

where ν is Poisson's ratio, E the Young's modulus, and ε_r^* the radial misfit strain arising from thermal anisotropy effects. Wear at the grain/matrix interface is simulated by adjusting ε_r^* to accommodate equal amounts of material being removed from either side of the interface during cycling, and is quantified in terms of a simple wear relationship, based on Amonton's Law, in terms of the normal stress at the interface, $\sigma_N = \sigma_R$, and the sliding distance, s. The volume of material removed, V, is given by [44]

$$V = \alpha \sigma_R s(\text{area}) \tag{5}$$

where α is the wear rate and area refers to the sliding contact area between the bridging grain and the matrix. Having developed equations which relate the amount of material removed at the grain/matrix interface to the change in misfit strain, ε_r^*, and the residual normal stress, σ_R, the frictional pullout function, $p(u)$, where $\sigma_N = \sigma_R$ (Equation 2), and subsequently the decrease in the shielding capacity of the zone, K_b, can be calculated [23]. Based on the computation of K_b, the near-tip driving force, K_{tip}, is determined from Equation 3, thereby providing a condition for crack growth at constant da/dN of the form $K_{tip} = K_0$, where K_0 is the intrinsic matrix toughness.

Growth rates in the three equiaxed aluminas (8, 10 and 13 μm) are seen generally to increase with decreasing grain size or fracture toughness (Fig. 8a), consistent with predictions from this frictional wear model. In grains with smaller dimensions, not only is shielding reduced, but removal of material at the bridge/matrix interface has a marked effect on reducing the misfit strain induced by thermal expansion anisotropy. As a result, the shielding capacity of the bridging zone is more sensitive to degradation via cyclic loading in smaller grained materials, and growth rates are therefore accelerated. This is borne out by the close comparison between the experimental growth-rate data for the 8 and 13 μm Al_2O_3 micro-

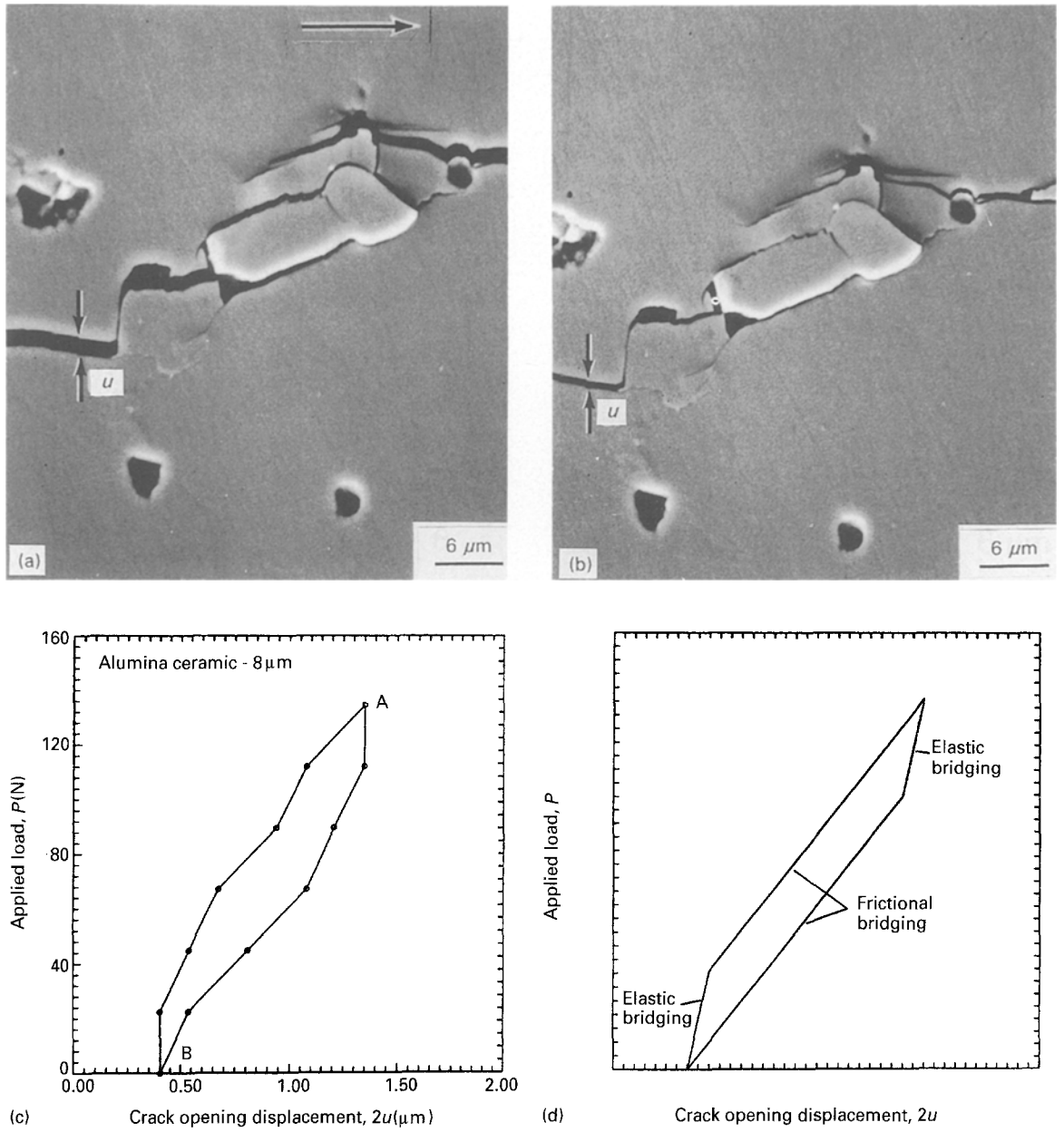

Figure 10 Scanning electron micrographs of a bridging grain in the profile of a fatigue crack ~ 2 mm behind the crack tip in the 8 μm grain-sized Al_2O_3 at (a) maximum load of applied cycle, and (b) zero load. Included are applied load, P, versus crack-opening displacement, $2u$, curves showing (c) measured, and (d) schematically illustrated hysteretic behaviour resulting from frictional sliding of bridging grains. Notice the residual crack opening at zero load, indicating the presence of closure.

structures and predictions from the above described frictional wear model (Fig. 13), calculated using the properties listed in Table I ($2u^* \approx d_{gs}$ which defines the bridging zone length, although as discussed elsewhere [23], the frictional-wear model is not sensitive to this length scale) and a wear rate, α, typical of alumina on alumina in air of 10^{-7} mm^3 N^{-1} m^{-1} [45].

3.2.3. Effect of load ratio

Growth rates are accelerated with increasing load ratio for the 8 μm grain-sized alumina when plotted in terms of ΔK (Fig. 14a). Although the slope, m, is essentially unchanged, the fatigue thresholds are decreased from ~ 2.3 MPa m$^{1/2}$ at $R = 0.1$ to ~ 1.8 MPa m$^{1/2}$ at $R = 0.5$. This variation in ΔK_{th} with R can essentially be normalized by plotting growth-rate data as a function of K_{max} (Fig. 14b). In fact, when Equation 1 is written in terms of both K_{max} and ΔK, i.e.

$$da/dN = C'(K_{max})^n(\Delta K)^p \quad (6)$$

where $C' = C(1 - R)^n$ and $(n + p) = m$, it is apparent that, unlike metals, growth rates in alumina show a far greater dependence upon K_{max} than ΔK. A regression fit to the data in Fig. 14 yields values for n and p of ~ 21.8 and 9.8, respectively; by comparison, values for a nickel-based superalloy are $n \sim 0.4$ and $p \sim 3$ [46]. Such observations that growth rates show a marked dependence on K_{max} and R and can be normalized by plotting in terms of K_{max}/K_c (Fig. 8b), together with the observed similarity between static and cyclic fracture surface morphologies, are consistent with the notion that the

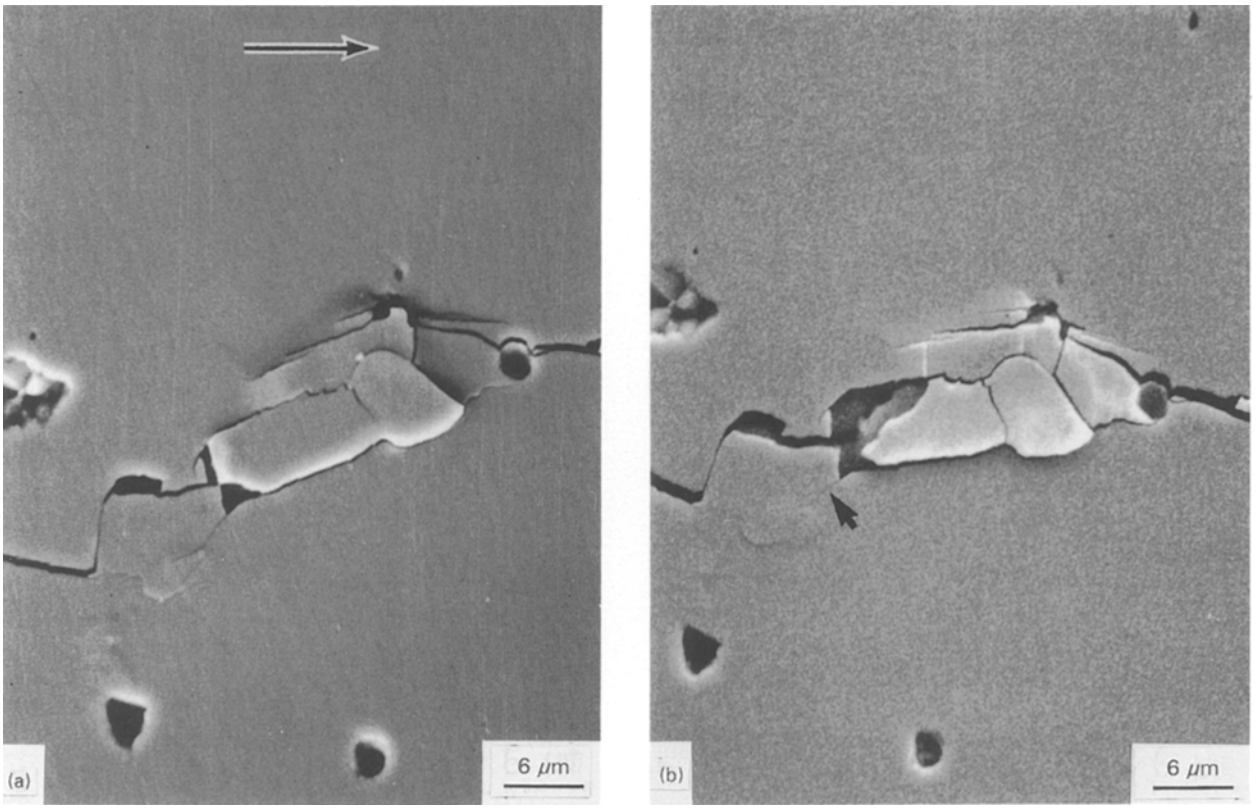

Figure 11 Scanning electron micrographs of a bridging grain in the 8 μm grain-sized Al_2O_3 (a) before and (b) after being subjected to $\sim 2 \times 10^6$ loading cycles ($R = 0.1$, $\nu = 25$ Hz). Degradation of the bridge is apparent. The secondary crack (marked with an arrow) has closed, indicating a reduction in the local frictional traction along the boundary. Horizontal arrow indicates direction of crack advance.

mechanisms associated with crack growth in ceramics (ahead of the crack tip) are similar for cyclic and static fatigue.

Of particular note here is that by plotting growth rates as a function of K_{max} (Fig. 14b), there is an apparent negative effect of load ratio, i.e. growth rates are accelerated with decreasing R at constant K_{max}. This can be anticipated by relating the effect of R (and hence, the applied ΔK) on the grain/matrix sliding distance, s, through consideration of the crack-opening profile, $2u(x)$, where $(a - x)$ is distance behind the crack tip (Fig. 9a). An edge-crack profile can be used to approximate the crack opening profile. Assuming small-scale yielding‡ (in this case, for a small-scale bridging zone length), the magnitude of the crack-opening displacements are fixed by the near-tip driving force, K_{tip}, such that [48]

$$2u(x) = \frac{\Psi K_{tip}}{E a^{1/2}}(a^2 - x^2)^{1/2} D\left(\frac{x}{a}\right) \quad (7)$$

where $\Psi \sim 2.1$, and $D(x/a)$ is a function dependent solely on x/a. The sliding distance per loading cycle, s, can subsequently be defined in terms of the maximum and minimum crack-opening displacements during the loading cycle, $2u(x)|_{K_{tip}^{max}}$ and $2u(x)|_{K_{tip}^{min}}$, as

$$s = 2u(x)|_{K_{tip}^{max}} - 2u(x)|_{K_{tip}^{min}} = \Delta[2u(x)] \quad (8)$$

This allows s to be expressed in terms of Equation 7 and the applied ΔK, i.e.

$$s = \Delta[2u(x)] = \frac{\Psi \Delta K_{tip}}{E a^{1/2}}(a^2 - x^2)^{1/2} D\left(\frac{x}{a}\right) \quad (9)$$

which reduces to

$$s = \frac{\Psi K_{tip}^{max}(1 - R)}{E a^{1/2}}(a^2 - x^2)^{1/2} D\left(\frac{x}{a}\right) \quad (10)$$

Inspection of Equation 10 indicates that an increased load ratio (at constant K_{max}) results in concurrent reduction of the sliding distance and boundary wear with each loading cycle (Equation 5); hence, as is consistent with experiments in Fig. 14b, growth rates decrease with increasing load ratio when plotted in terms of K_{max}.

However, observations of high levels of crack closure of up to 50% of K_{max} in the 10 μm alumina

‡ Because the profile is greatly influenced by the nature of the grain-bridging stress function, $p(u)$, as well as on specimen geometry and loading configuration, proper formulation of the bridged crack problem requires numerical solutions to an integral equation [47]. This approach is mathematically complex, however, and the shape of the profile is often assumed a priori to simplify calculations [42].

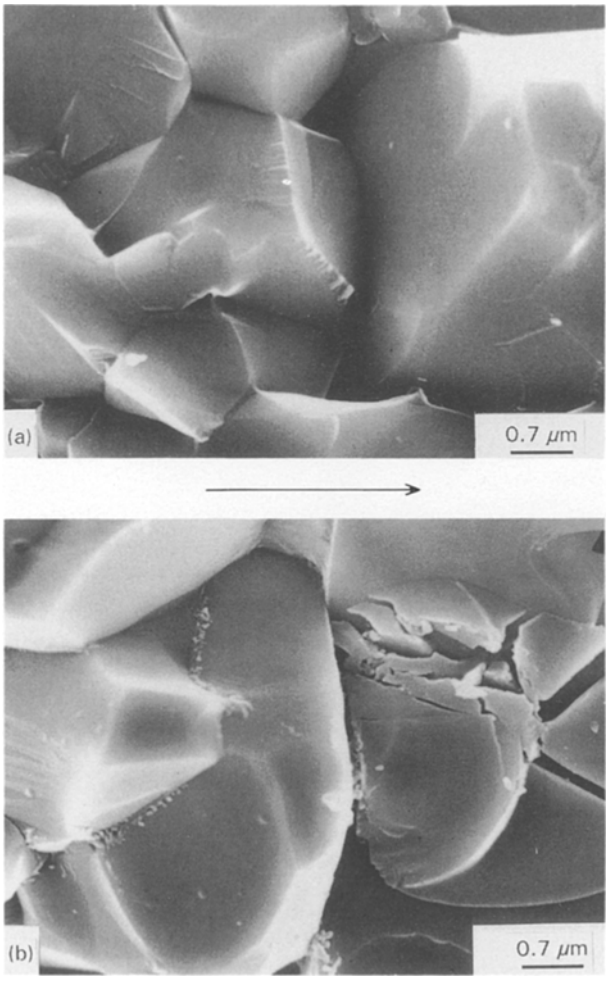

Figure 12 Scanning electron micrographs of fracture surfaces broken under (a) monotonic, and (b) cyclic loading conditions in the Coors 99.5% pure Al_2O_3. While the morphology of the surfaces is very similar (unlike analogous surfaces in a metal), evidence of damage exists on the fatigue surface which is not as readily observed on the monotonic surface. Arrow indicates direction of crack advance.

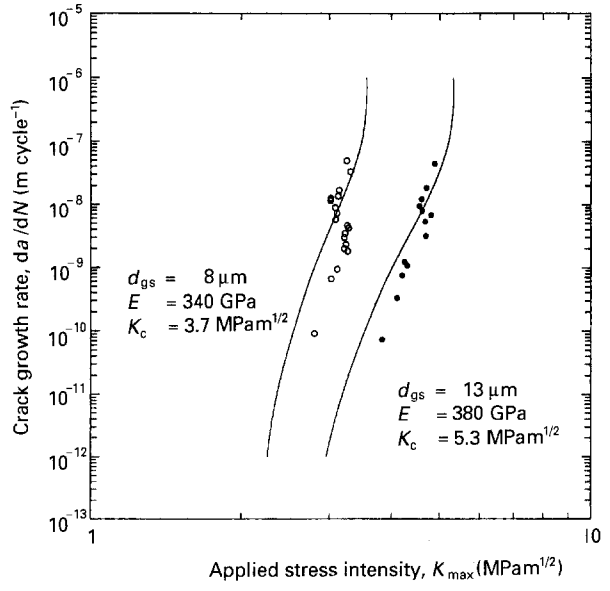

Figure 13 Comparison of measured and predicted cyclic fatigue-crack growth rates, da/dN, in the 8 and 13 μm grain-sized aluminas as a function of the applied K_{max} ($R = 0.1$) using frictional wear model [23].

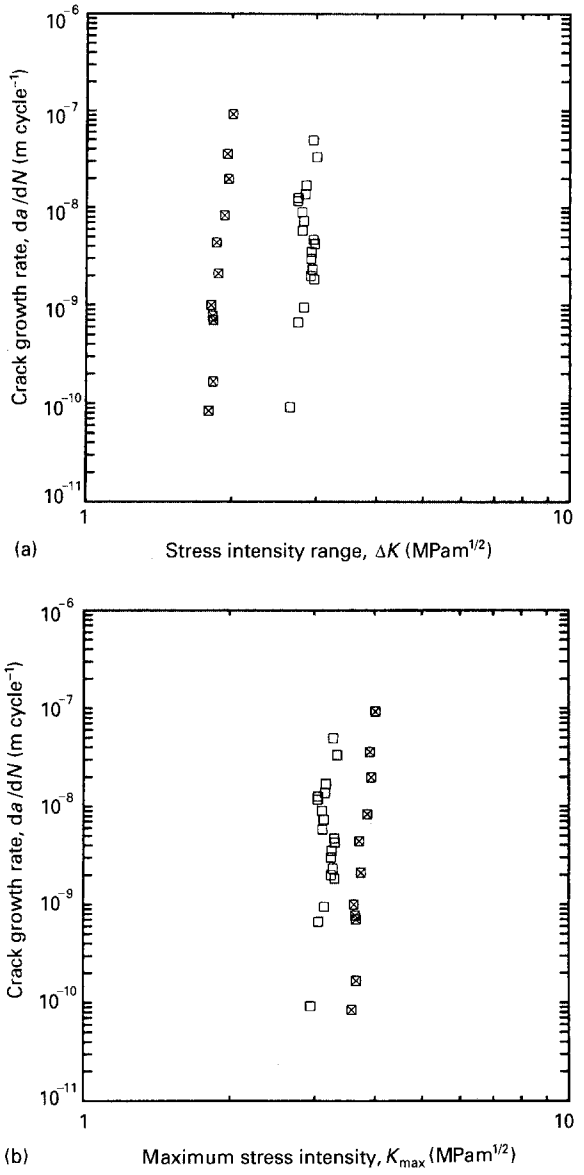

Figure 14 Effect of load ratio (R = (□) 0.1 and (⊠) 0.5, ν = 25 Hz) on the cyclic fatigue-crack growth rate, da/dN, behaviour of the 8 μm grain-sized alumina, plotted in terms of (a) ΔK, and (b) K_{max}. Notice the closer normalization of the data in (b), indicating a large growth-rate dependence on K_{max} relative to ΔK.

(Fig. 15) have not been accounted for. These measurements are consistent with the large degree of residual crack opening (e.g. Fig. 10b) resulting from premature contact of rough asperities on the fracture surfaces; interference between such asperities presumably arises from processes such as crack-tip shear displacements, wear debris, and stress relaxation. While it is widely understood that closure has marked effects on cyclic crack-growth rates in metals due to a local decrease in the effective stress-intensity range experienced at the crack tip (i.e. $\Delta K_{eff} = K_{max} - K_{cl}$, where $K_{cl} > K_{min}$ [49, 50]), the role of closure in ceramic fatigue is still poorly understood. By reducing the boundary sliding distance at the bridge/matrix interface, it is conceivable that closure abates the severity of bridge degradation during cyclic loading, thereby retarding growth rates in alumina as it does in metals. Because of the relatively small dependence of growth rates on ΔK, however, this effect is not expected to play as

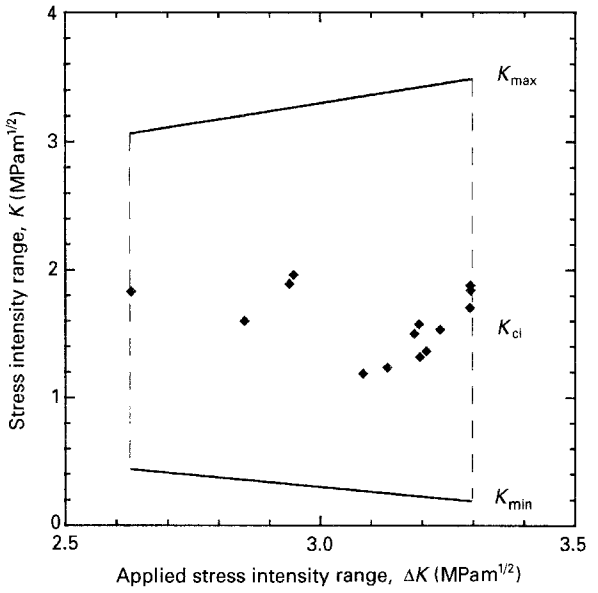

Figure 15 Measured variation in the stress intensity at crack closure, K_{cl}, with applied ΔK, in the 10 μm Al_2O_3 during cyclic loading. Applied values of K_{max} and K_{min} are shown for comparison. Note the large closure levels, approaching ~ 50% of K_{max}.

significant a role in alumina. The phenomenon is also obscured by the presence of bridging in ceramic materials, which makes the interpretation of closure difficult. Despite these difficulties, indications of extensive damage and micro-fracture of bridging elements observed at various sites along cyclically grown crack paths and the observed debris on fatigue fracture surfaces are consistent with the measured closure levels.

4. Conclusions

1. Rates of subcritical crack growth under cyclic loads are observed to be many orders of magnitude faster than corresponding growth rates under monotonic loading at equivalent stress intensity levels for each of the five Al_2O_3 microstructures.

2. Cyclic fatigue-crack growth is rationalized in terms of a reduction in the shielding capacity of grain-bridging zones due to frictional wear at the bridge/matrix boundaries. Such degradation is consistent with *in situ* SEM observation of load versus crack-opening displacement hysteresis loops, damage to active bridging sites, and wear debris on fatigue fracture surfaces.

3. Cyclic fatigue-crack growth rates are accelerated by a reduction in grain size. This can be rationalized in terms of the removal of grain-boundary material due to wear along bridge/matrix interfaces and the subsequent reduction in thermal expansion misfit strain. Not only is sheilding reduced for smaller grain sizes, but, the removal of boundary material more rapidly reduces the misfit strain in smaller grained aluminas, and so enhances cyclic crack advance.

4. The large growth-rate dependence on K_{max} is a result of the dominance of static failure modes on crack advance in both monotonic *and* cyclic subcritical crack growth. The smaller ΔK dependence stems from the importance of frictional sliding wear (which scales directly with ΔK) on the degradation of the crack-tip shielding zone, a process which enhances the crack-tip driving force. At constant K_{max}, a higher load ratio leads to lower growth rates due to a commensurate reduction in the bridge/matrix sliding distance.

5. High levels of crack closure, approaching ~ 50% of K_{max}, were measured, consistent with the observed damage to bridging elements and fatigue fracture surfaces during cyclic loading. While this effect is not accounted for in any of the frictional wear models for crack growth, it presumably limits the range of bridge/matrix sliding and subsequently the amount of wear per loading cycle.

6. The observed dependence of cyclic crack-growth rates on mechanical and microstructural variables, such as load ratio and grain size, and fractographic and *in situ* crack path analyses, are consistent with a mechanism for crack advance in alumina involving the degradation of crack-tip shielding by grain bridging due to cyclically induced wear along the grain/matrix interfaces.

Acknowledgement

This work was suppoprted by the US National Science Foundation under Grant DMR-9123279.

References

1. S. M. WIEDERHORN, B. J. HOCKEY and D. E. ROBERTS, *Philos. Mag.* **28** (1973) 783.
2. L. S. WILLIAMS, *Trans. Br. Ceram. Soc.* **55**(5) (1956) 287.
3. B.K. SARKAR and T. G. T. GLINN, *ibid.* **69**(5) (1970) 199.
4. D. A. KROHN and D. P. H. HASSELMAN, *J. Am. Ceram. Soc.* **55** (1972) 208.
5. F. GUIU, *J. Mater. Sci. Lett.* **13** (1978) 1357.
6. E. B. SHAND, *Am. Ceram. Soc. Bull.* **38** (1959) 653.
7. A. G. EVANS and E. R. FULLER, *Metall. Trans.* **5** (1974) 27.
8. R. O. RITCHIE and R. H. DAUSKARDT, *J. Ceram. Soc. Jpn* **99** (1991) 1047.
9. S. HORIBE and R. HIRAHARA, *Acta Metall. Mater.* **39** (1991) 1309.
10. T. HOSHIDE, T. OHARA and T. YAMADA, *Int. J. Fract.* **37** (1988) 47.
11. F. GUIU, M J. REECE and D. A. J. VAUGHAN, *J. Mater. Sci.* **26** (1991) 3275.
12. H. KISHIMOTO, *JSME Int. J.* **34** (1991) 393.
13. S. SURESH, *J. Hard Mater.* **2** (1991) 29.
14. F. GUIU, M. LI and M. REECE, *J. Am. Ceram. Soc.* **75** (1992) 2976.
15. S. LATHABAI, Y. MAI and B. LAWN, *ibid.* **72** (1989) 1760.
16. T. KAWAKUBO and K. KOMEYA, *ibid.* **70** (1987) 400.
17. R. KNEHANS and R. STEINBRECH, *J. Mater. Sci. Lett.* **1** (1982) 327.
18. P. BECHER, *J. Am. Ceram. Soc.* **74** (1991) 255.
19. S. J. BENNISON and B. R. LAWN, *Acta Metall. Mater.* **37** (1989) 2659.
20. A. G. EVANS and K. T. FABER, *J. Am. Ceram. Soc.* **67** (1984) 255.
21. R. M. McMEEKING and A. G. EVANS, *ibid.* **65**.(1982) 242.
22. J. RÖDEL, *J. Eur. Ceram. Soc.* **9** (1992) 323.
23. R. H. DAUSKARDT, *Acta Metall. Mater.* **41** (1993) 2765.
24. S. LATHABAI, J. RÖDEL and B. LAWN, *J. Am. Ceram. Soc.* **74** (1991) 1360.
25. P. L. SWANSON, C. J. FAIRBANKS, B. R. LAWN, Y-W. MAI and B. J. HOCKEY, *ibid.* **70** (1987) 279.
26. J. RÖDEL, J. KELLY and B. LAWN, *ibid.* **73** (1990) 3313.

27. G. VEKINIS, M. F. ASHBY and P. W. R. BEAUMONT, *Acta Metall. Mater.* **38** (1990) 1151.
28. H. E. LUTZ, X. Z. HU and M. V. SWAIN, *J. Eur. Ceram. Soc.* **9** (1992) 133.
29. Y. MANIETTE, M. INAGAKI and M. SAKAI, *ibid.* **7** (1991) 255.
30. D. C. SALMON and D. W. HOEPPNER, in "Second Symposium on Cyclic Deformation, Fracture, and Nondestructive Evaluation of Advanced Materials," Miami, November 1992, edited by M. R. Mitchell and O. Buck, STP 1184 (American Society for Testing and Materials, Philadelphia, PA, 1994).
31. C.-W. LI, D.-J. LEE and S.-C. LUI, *J. Am. Ceram. Soc.* **75** (1992) 1777.
32. A. G. EVANS, *Mater. Sci. Eng.* **A143** (1991) 63.
33. H. CAI, K. T. FABER and E. R. FULLER, Jr, *J. Am. Ceram. Soc.* **75** (1992) 3111.
34. J. C. HAY and K. W. WHITE, *ibid.* **76** (1993) 1849.
35. T. TANAKA, N. OKABE and Y. ISHIMARU, *J. Soc. Mater. Sci. Jpn* **38** (1989) 137.
36. D. ROUBY and P. REYNAUD, *Compos. Sci. Technol.* **48** (1993) 109.
37. R. H. DAUSKARDT and R. O. RITCHIE, *Closed Loop* **17** (1989) 7.
38. R. O. RITCHIE and W. YU, in 'Small Fatigue Cracks", edited by R. O. Ritchie and J. Lankford (The Metallurgical Society of the American Institute of Mining, Metallurgical and Petroleum Engineers, Warrendale, PA, 1986) p. 167.
39. H. N. KO, *J. Mater. Sci. Lett.* **5** (1986) 464.
40. *Idem, ibid.* **8** (1989) 1438.
41. P. C. PARIS and F. ERDOGAN, *J. Bas. Eng. Trans. ASME* **85** (1963) 528.
42. Y. W. MAI and B. R. LAWN, *J. Am. Ceram. Soc.* **70** (1987) 289.
43. A. G. EVANS and R. M. McMEEKING, *Acta Metall. Mater.* **34**(12) (1986) 2435.
44. T. E. FISCHER, M. P. ANDERSON, S. JAHANMIR and R. SALHER, in "Wear of Materials 1987", Vol. 1, edited by K. C. Ludema (ASME, New York, 1987) p. 257.
45. N. WALLBRIDGE, D. DOWSON and E. W. ROBERTS, in "Wear of Materials 1983", edited by K. C. Ludema (ASME, New York, 1983) p. 202.
46. R. H. VanSTONE, *Mater. Sci. Eng.* **A103** (1988) 49.
47. B. N. COX and D. B. MARSHALL, *Acta Metall.* **39** (1991) 579.
48. H. TADA, P. C. PARIS and G. R. IRWIN, "The Stress Analysis of Cracks Handbook", Part III (Paris Productions, St Louis, 1985).
49. W. ELBER, *Eng. Fract. Mech.* **2** (1970) 37.
50. S. SURESH and R. O. RITCHIE, in "Fatigue Crack Growth Threshold Concepts", edited by S. Suresh and D. L. Davidson (The Metallurgical Society of the American Institute of Mining, Metallurgical and Petroleum Engineers, Warrendale, PA, 1984) p. 227.

Received 13 April
and accepted 16 May 1994